Model-to-image based 2D-3D-registration of angiographic data

Sabine Mollus[a], Jördis Lübke[b], Andreas J. Walczuch[a], Heidrun Schumann[c], Jürgen Weese[a]

[a]Philips Research Europe, Weisshausstr. 2, D-52066 Aachen, Germany
[b]University Medical Center Freiburg, Hugstetterstr. 55, D-79016 Freiburg, Germany
[c]University of Rostock, Albert-Einstein-Str. 21, D-18051 Rostock, Germany

ABSTRACT

We propose a novel registration method, which combines well-known vessel detection techniques with aspects of model adaptation. The proposed method is tailored to the requirements of 2D-3D-registration of interventional angiographic X-ray data such as acquired during abdominal procedures. As prerequisite, a vessel centerline is extracted out of a rotational angiography (3DRA) data set to build an individual model of the vascular tree. Following the two steps of local vessel detection and model transformation the centerline model is matched to one dynamic subtraction angiography (DSA) target image. Thereby, the in-plane position and the 3D orientation of the centerline is related to the vessel candidates found in the target image minimizing the residual error in least squares manner. In contrast to feature-based methods, no segmentation of the vessel tree in the 2D target image is required. First experiments with synthetic angiographies and clinical data sets indicate that matching with the proposed model-to-image based registration approach is accurate and robust and is characterized by a large capture range.

Keywords: 2D-3D-registration, image guided interventions, X-ray angiography, TACE

1. INTRODUCTION

A rising number of catheter based abdominal interventions, such as the transarterial chemoembolization (TACE), rely on rotational imaging with C-arm based X-ray systems. In addition to a standard projection series, such as dynamic subtraction angiography (DSA), a rotational angiography (3DRA) is obtained to visualize the topology and the inflow of contrast agent into the vessel tree of interest in three dimensions.

Many treatment decisions require that the physician establishes the correspondence between the different angiographic data sets in his mind. This can be a challenging task, since the image data that is acquired during the intervention is commonly affected by motion. Especially abdominal images are prone to deformations caused by breathing, heart beat, swallowing and peristaltic movements. Even the blood pulse and the interventional devices themselves can displace parts of the studied vessel tree to a certain amount. In addition, vascular images often present alignment ambiguities due to topologically similar sub-trees and due to the varying degree of vascular enhancement, which is dependent on the position of the contrast agent injection. Furthermore, the acquisition geometry is typically changed between two acquisitions. Hence, the correspondence between a rotational angiography and a DSA sequence can be limited so that the correct alignment requires experience and a trained eye.

Automatic 2D-3D-registration in combination with sophisticated visualization and overlay techniques can help to transfer information from the three-dimensional acquisition to the two-dimensional data. This facilitates treatment planning as well as navigation of the interventional devices to the treatment site. Different methods for 2D-3D-registration of angiographic data have been proposed. They can be categorized as intensity-based, feature-based, reconstruction-based and hybrid methods.

Intensity-based methods such as those presented in[1–5] rely on digitally reconstructed radiographs (DRR). DRRs are simulated X-ray images obtained from the 3D reference angiography that, during registration, are related to the target X-ray image using specific similarity measures. Since vessels are rather linear structures and vessel trees are often symmetric, it is difficult to define a discriminative similarity measure that can distinguish between a local, sub-optimal overlap of vessel structures and a global, optimal matching. Hence, often the

Medical Imaging 2008: Image Processing, edited by Joseph M. Reinhardt, Josien P. W. Pluim,
Proc. of SPIE Vol. 6914, 69142S, (2008)
1605-7422/08/$18 · doi: 10.1117/12.770025

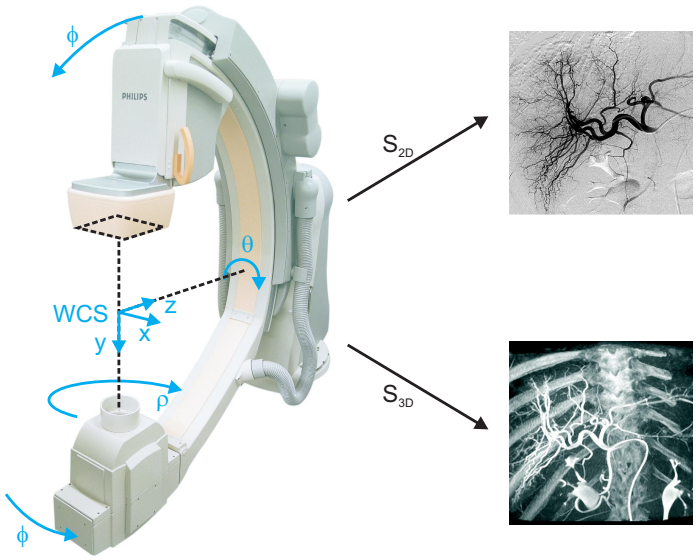

Figure 1. Registration set-up and the six degrees of freedom of the rigid-body 2D-3D-registration problem. The origin of the world coordinate system (WCS) is linked to the center of the reconstructed 3DRA volume. The coordinate systems of the reference volume $\mathbf{S}_{3D}$ and the target image $\mathbf{S}_{2D}$ are well-defined by the intrinsic system parameters

resulting optimization landscape is not convex and the capture range is limited[6]. To our knowledge, no intensity-based method has been successfully validated for abdominal data.

Recently, Groher et al.[7] and Jomier et al.[8] proposed different feature-based 2D-3D-registration approaches for abdominal applications. In general, feature-based methods[3,6,9–12] rely on the extraction of the vessel tree in the 3D and the 2D data set. Iteratively, the distance between the segmented 2D primitives and the projection of the 3D features is minimized. However, registration quality of feature-based methods depends on the accuracy of the segmentation, which is a challenging task in itself. Since the point-to-point based correspondence built up during registration is often imperfect, the registration process is easily locked by a small set of misaligned points. To reduce the influence of outliers, Groher et al.[13] developed a method that systematically removes non-corresponding features in the 2D and the 3D data set.

Reconstruction-based methods, such as proposed in[14], build up a 3D vessel tree from multiple 2D views of the object of interest. Then 3D-3D-registration techniques are applied to align the reconstructed vessel tree to the second 3D data set. The main drawback of this method is the poor quality of the reconstructed vessel tree, which can hamper registration. Furthermore, interventional images from different views are required, which is a serious limitation for clinical use.

We introduce a hybrid approach of model-to-image based 2D-3D-registration. The basic idea is to use matching techniques known from model-based segmentation[15] to align a given geometrical model of the vascular tree to a planar target image. In contrast to feature-based methods, it is not required to segment the vessel tree in the 2D data set. This makes the registration more efficient, more flexible and in many cases increases the degree of correspondence.

2. METHOD

In the first step of 2D-3D-registration, the coordinate system of the 3DRA reference data set $\mathbf{S}_{3D}$ has to be aligned to the coordinate system of the 2D target acquisition $\mathbf{S}_{2D}$, as illustrated in Fig. 1. Since the C-arm based X-ray system is well calibrated, all intrinsic parameters for the geometrical registration are known. However, due to peri-interventional motion this purely geometry-based transformation is typically not sufficient to accurately align the object of interest in the 2D and 3D data set to each other. Hence, the goal of 2D-3D-registration is to find a transformation T that relates the reference data set to the target set more precisely.

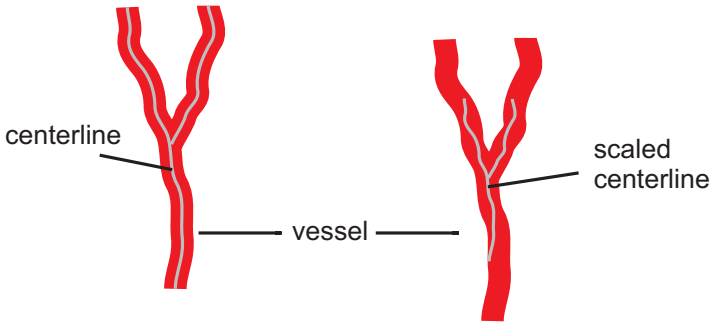

Figure 2. Example of scaling invariance. Since vessels are rather linear structures and vessel trees are often symmetric, the off-plane translation t_y can be difficult to optimize for a 2D-3D-registration algorithm. Thus, in this study, the influence of t_y is neglected. This is no major restriction when dedicated means to fine-tune the off-plane translation interactively or to continuously track the table position during the intervention are provided. In addition, the in-plane translations and rotations are more important, as already indicated in[13].

Assuming that a rigid transformation is sufficient to correct for the misalignments of the object of interest in the 2D and the 3D data set, the given registration problem can be expressed as follows:

$$T(\tilde{\mathbf{x}}_i) = \mathbf{R}_\rho \mathbf{R}_\phi \mathbf{R}_\theta \tilde{\mathbf{x}}_i + \mathbf{t}. \tag{1}$$

The transformation T is described by six extrinsic parameters: the 3D translational parameters $\mathbf{t} = [t_x t_y t_z]$, which are defined with respect to the axes of the world coordinate system (WCS), and the three rotation angles θ, ϕ, ρ, that correspond to the primary angle, the secondary angle and the L-arm position of the C-arm system. In the first version of the proposed algorithm, the influence of the off-plane translation t_y is neglected. Figure 2 illustrates that this parameter is critical to optimize due to the inherent scaling invariance of linear and symmetrical objects such as certain vessels.

As a prerequisite of the proposed model-based registration method, the vessel centerline of interest $\{\tilde{\mathbf{x}}_i\}$ has to be extracted from the reference volume. Therefore, we use well-known vessel segmentation[16,17], thinning[18], modeling and pruning techniques[19]. Additionally, a target image has to be gathered from a DSA series. Then matching is performed following the two steps of local vessel detection and model transformation.

2.1 Local vessel detection

To establish correspondences between the reference model and the target image, the forward projection $P(\tilde{\mathbf{x}}_i) = \mathbf{x}_i$ of the centerline is computed and used for local vessel detection. Starting from each projected centerline element $\mathbf{x}_i$, a search is cast along a predefined direction such as the centerline's normal $\mathbf{n}_i$ to find the target point

$$\mathbf{x}_i^{l_i} = \mathbf{x}_i + l_i \delta \mathbf{n}_i \tag{2}$$

$$\hat{\mathbf{x}}_i = \min_{\{\mathbf{x}_i^{l_i} | l_i = -L \ldots L\}} \{\lambda l_i^2 + F_i(\mathbf{x}_i^{l_i}, \mathbf{n}_i)\}. \tag{3}$$

The location of $\hat{\mathbf{x}}_i$ is the point with the optimal combination of feature value $F(\mathbf{x}_i^{l_i}, \mathbf{n}_i)$ and distance l_i to the projected centerline. The parameter λ is an arbitrary value, which penalizes vessel candidates that are far away from the current centerline position, L defines the length of the profile investigated, and the parameter δ denotes the distance between two neighbored points on the surveyed profile. The basic principle of local vessel detection is illustrated in Fig. 3.

The choice of the feature function F is essential for robust registration. Basically, the feature function should have a small cost at a vessel centerline and a high cost at other locations. A common feature function for vessel detection makes use of the predominately elliptical shape of the blood vessel lumen. Assuming that the concentration of the contrast agent does not vary spatially, and the relationship between the measured image

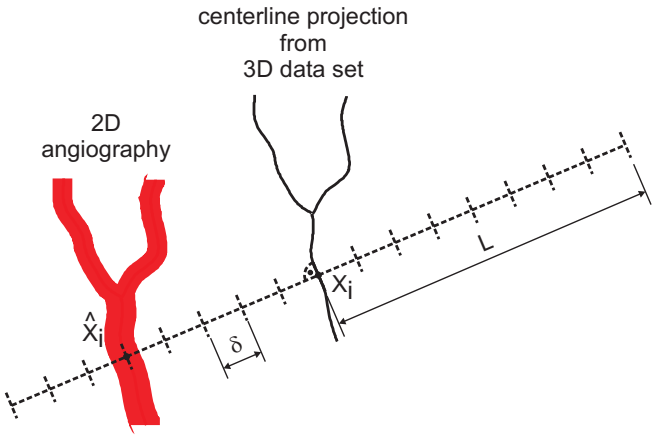

Figure 3. Principle of local vessel detection. Perpendicular to each element of the projected reference vessel centerline a search profile is defined. Along the search profile, a vessel cross-section model is matched to identify the corresponding vessel in the target image

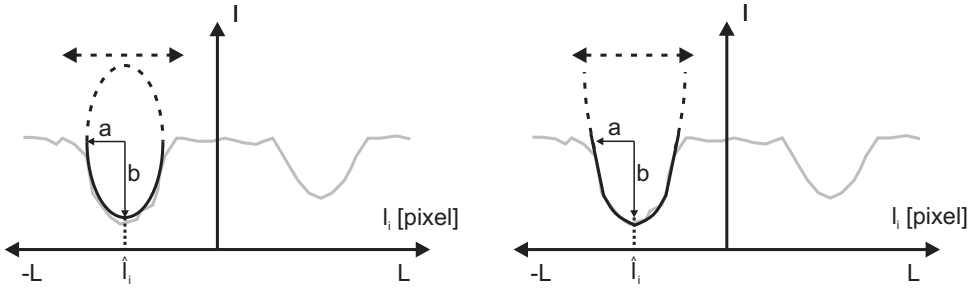

Figure 4. Adaptation of different cross-section models for target point search. Along a search profile, a vessel cross-section model is shifted and matched to the underlying data. Different test functions can be used, for example an ellipse model (left) or a quadratic function (right)

intensities and the local X-ray absorption is known, a vessel typically appears as an elliptically shaped *valley* in the densitometric profile[20, 21]. Alternatively, a Gaussian-type model, a quadratic or a piece-wise defined test function can be used to approximate the shape of a vessel in a cross-section view.

To identify a target point, the selected model is shifted over the search profile. As illustrated in Fig. 4, the position and the free parameters of the test function, such as the length of the major and minor axis of the ellipse model or the polynomial coefficients of the quadratic function, have to be optimized. For optimization, the mean-squared error between the test function and the underlying part of the gray value profile is computed. To restrict the free parameters of the test function to a proper range, the characteristics of the 3D reference vessel model such as the typical vessel radii of the hepatic vessel tree are considered. Finally, the feature function F is given by the mean squared error of the best matching result or remains undefined, when no vessel candidates could be found.

2.2 Model transformation and optimization

The second step of model-based registration involves finding the optimal position and orientation that relates the reference centerline to the destination image. In analogy to the external energy used in the context of model-based segmentation, we define a metric that penalizes the difference between the transformed and projected centerline $\{P(T(\tilde{\mathbf{x}}_i))\}$ and the target point list $\{\hat{\mathbf{x}}_i\}$

$$E^k = \sum_i w_i^k (P(T^k(\tilde{\mathbf{x}}_i)) - \hat{\mathbf{x}}_i^k)^2. \tag{4}$$

Illustratively, this describes the attraction of a centerline element with an elastic spring to the target point. The contribution of each centerline element can be biased with a specific weight $w_i \in \mathbf{w}$. A more advanced version of the external energy is based on the observation that directly attracting centerline elements tends to keep target points fixed in subsequent iterations. Thus, a tangent $\mathbf{m}$ along the vessel centerline at the target point is devised. It attracts a centerline element, allowing the centerline to move away from the selected target point along $\mathbf{m}$. Formally, this is written as

$$E^k = \sum_i w_i^k (\mathbf{m}_i (P(T^k(\tilde{\mathbf{x}}_i)) - \hat{\mathbf{x}}_i^k))^2. \tag{5}$$

To obtain $\mathbf{m}$, e.g. an eigenvector analysis of the Hessian matrix according to[22] can be applied to the target image.

Typically, one matching step between the reference centerline and the target point list is not sufficient. In fact, an initial estimate of the transformation T^0 has to be gradually refined in a series of iterations. In each iteration k, an update of the target point list is generated and a new transformation is computed. We propose a heuristic approach that, in the first stage, starts the optimization with a small number of registration parameters. In the next stage, the solution of this lower-order problem is used to solve the registration problem for further degrees of freedom. To our observations, the most prominent differences between the 2D and the 3D data sets are commonly due to translations. Hence, in analogy to[1], we first try to retrieve a rough estimate of these extrinsics before the rotation parameters θ, ϕ, ρ are added to the optimization process. During each optimization step, Eq. (5) is minimized using the Levenberg-Marquardt algorithm[23, 24].

3. EXPERIMENTAL DATA AND EXPERIMENTS

We evaluated the accuracy and the robustness of the proposed registration algorithm in two simulation studies and for two clinical data sets.

3.1 Clinical data

The clinical data sets were obtained from two patients who were treated for liver cancer with TACE. The data sets were acquired on a Philips Allura FD20 X-ray system. For validation, a 3D rotational angiography (volume dimension $256 \times 198 \times 256$, voxel size $0.99 \times 0.99 \times 0.99$ mm^3) and a single frame from a DSA sequence (image dimension 1024×1024, pixel size 0.308×0.308 mm^2) were selected. The DSA sequence was acquired from the anterior-posterior perspective as it is typical for the TACE application. The location of contrast agent injection in both data sets was selective.

Figure 5 shows the DSA frames selected for registration for both patients. Furthermore, the centerlines, which were extracted from the respective 3DRA data sets and projected according to the intrinsic and extrinsic settings of the 2D target acquisition, are overlaid to the DSA frame. These examples illustrate the main challenges for 2D-3D-registration. First, the geometrical alignment is far away from the optimum which is the cause of patient motion, unknown patient thickness and interventional table movements that were not tracked. Second, the correspondence between both data sets is limited due to non-rigid deformations, the different degree of angiographic enhancement and imperfections of the 3D vessel segmentation.

As no ground truth registration is available for these clinical data sets, the reference parameter set was obtained from a manual registration. The quality of the manual registration can be assessed in Fig. 5.

3.2 Synthetic data

In addition, a simulation study was performed to evaluate the proposed registration algorithm with respect to a well-defined ground truth. The basic idea of this study was to synthetically generate appropriate DSA sequences using the 3D reference angiography as prototype. The geometrical relation between the synthetic DSA sequence and the 3D reference can be set up using the cone-beam projection geometry of the C-arm. In this approach, the ground truth registration between both data sets is simply defined by the extrinsic and intrinsic parameters of the chosen projection function.

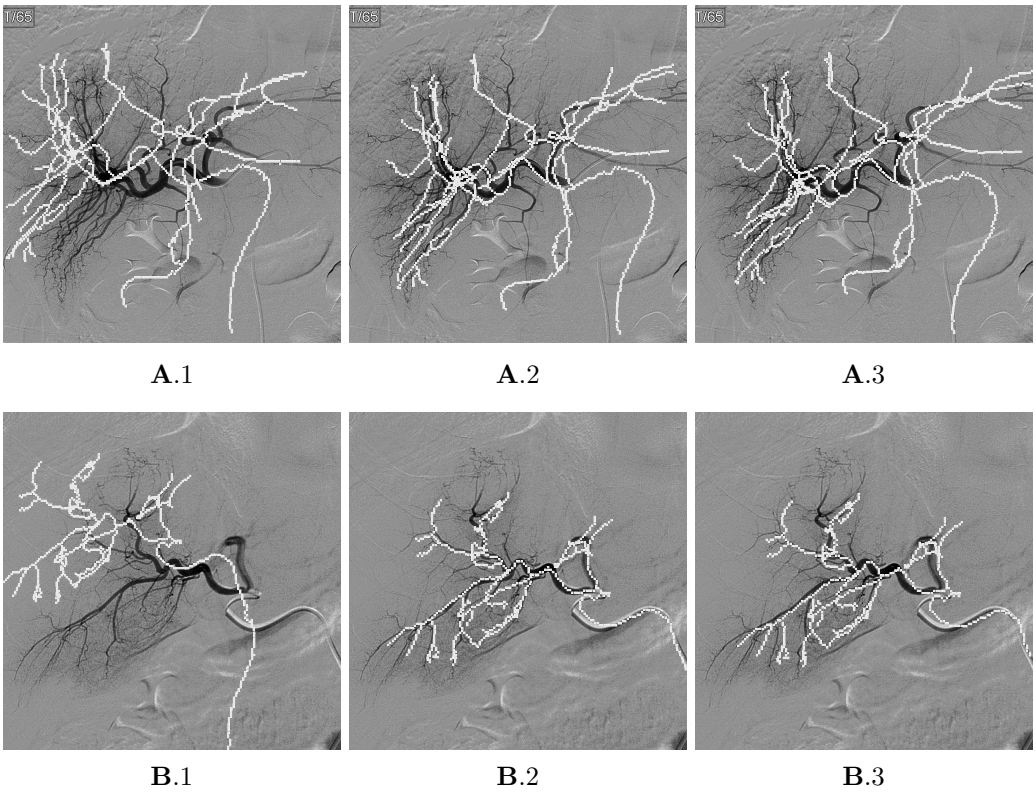

Figure 5. Registration examples with representative clinical data sets acquired during TACE procedure, (**A.1**) projected 3D centerline and target DSA image after geometrical matching, (**A.2**) manual reference registration, (**A.3**) typical registration result; (**B.1**) projected 3D centerline and target DSA image after geometrical matching, (**B.2**) manual reference registration, (**B.3**) typical registration result

To obtain realistic 2D angiographic data, a flow simulation according to[25] was performed. In the first step, a rotational X-ray data set is processed to extract the centerline as outlined in Sec. 2. In addition, information on the local vessel diameter has to be collected along the reference centerline. Similar to[20], we reconstruct the local vessel lumen from the projection series that is gathered for the 3DRA acquisition. Using the centerline and the diameter estimations, a 3D vessel model consisting of a set of tubes is constructed. Through this set of tubes, a simulation of volumetric blood flow following the rules of Hagen-Poiseuille is performed. The result is a 3D+t data set. Applying a ray-casting technique for a predefined projection geometry, this simulation can be condensed to a 2D synthetic angiography sequence. For our experiments, a maximum projection DSA frame was computed, where each pixel was set to the maximum level of contrast in that pixel over the sequence. The resulting target image includes overlap and foreshortening and is realistic with respect to the clinically relevant vessel topology and the local contrast agent distributions.

For the two clinical data sets presented in the previous section, Fig. 6 shows a maximum-intensity projection (MIP) of the 3D reference data set, the respective 3D centerline, the 3D vascular tube model and the resulting synthetic DSA frame. To define the gold-standard registration T_{gold}, a cone-beam projection from anterior-posterior viewing angle was assumed during DSA generation.

3.3 Evaluation methodology and experiments

In literature[26], commonly different metrics are used to quantify the quality of the 2D-3D-registration result with respect to the given ground truth. A widely used 3D error measure is the target registration error (TRE), which is the distance between the given point transformed with the registration T_{reg} and the same point transformed

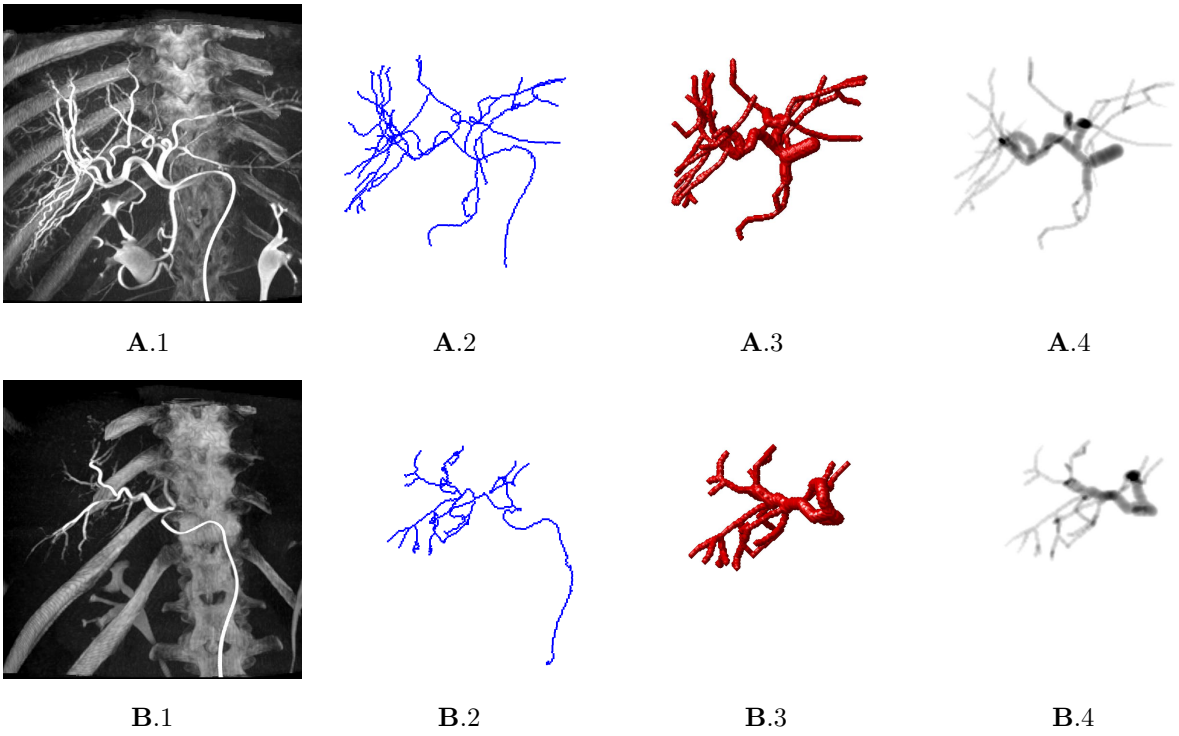

A.1 **A**.2 **A**.3 **A**.4

B.1 **B**.2 **B**.3 **B**.4

Figure 6. Ground truth data sets generated for the validation of the 2D-3D-registration algorithm. (**A.1**) MIP of clinical 3DRA reference data set, (**A.2**) reference vessel centerline, (**A.3**) 3D vessel model as result from vessel segmentation (the catheter was manually removed from the data set), (**A.4**) synthetic angiographic target image; (**B.1**) MIP of clinical 3DRA reference data, (**B.2**) reference vessel centerline, (**B.3**) 3D vessel model, (**B.4**) synthetic angiographic image

with the ground truth registration T_{gold}. The average distance between these point-pairs defines the mean target registration error (mTRE)

$$\text{mTRE}(\tilde{\mathbf{x}}, T_{\text{reg}}, T_{\text{gold}}) = \frac{1}{n}\sum_{i}^{n} ||T_{\text{reg}}(\tilde{\mathbf{x}}_i) - T_{\text{gold}}(\tilde{\mathbf{x}}_i)||. \tag{6}$$

For our application, the mTRE is computed for the set of centerline elements $\{\tilde{\mathbf{x}}_i\}$ of the reference model.

To assess the accuracy, the success rate and the capture range of the proposed algorithm, registration experiments from various starting positions were performed. In this study, per data set, 250 starting positions were derived from the respective ground truth registration. The transformation parameters are chosen randomly using independent, normally distributed variates. The parameters of the normal distribution can be retained from Table 1. Note that for the first evaluation of the proposed algorithm the influence of the off-plane translation t_y was neglected.

In the next step, the mTRE is computed for each of the randomly defined transformations. This 3D error is a measure of the starting distance to the reference registration and is used to uniformly distribute the matching experiments into intervals from 0–100 mm of initial mTRE. In this study, the range of the starting distances was divided into 10 subintervals each with a width of 10 mm. This means that 25 experiments were assigned to each evaluation bin. Each registration was classified as successful if the mTRE after registration was smaller than a predefined threshold of 5 mm. The registration accuracy was defined as the average mTRE value of all successful registrations. In analogy to[26], the capture range was expressed as the distance from the ground truth to the first subinterval for which the registration was successful in less than 95 % of the cases. In total, 1000 registration experiments were performed to evaluate the two synthetic and the two clinical data sets with regard to the given reference transformation.

Table 1. Parameters of Monte-Carlo based validation. According to the evaluation methodology introduced by[26], starting positions for the studied 2D-3D-registration algorithm are randomly defined. To each registration parameter a normally distributed variate is assigned that is defined by the mean value and its standard deviation. In addition, cut-off values are specified to limit the experiments to a relevant range of transformations

Registration parameters	μ_N	σ_N	min	max
t_x	0 mm	70 mm	-100 mm	100 mm
t_y	0 mm	0 mm	0 mm	0 mm
t_z	0 mm	70 mm	-100 mm	100 mm
θ	0°	10°	-15°	15°
ϕ	0°	10°	-15°	15°
ρ	0°	10°	-15°	15°

3.4 Implementation details

In this study, for local vessel detection, a quadratic test function as depicted in Fig. 4 is considered. According to our findings, the quadratic model yields a good compromise between detection quality and computational effort. Moreover, a binary weighting technique was chosen for the measurement of the registration energy as defined in Eq. (5). This technique sets $w_i = 1$, when the local target point search was successful, and $w_i = 0$ if no target point was found.

To steer the convergence of our optimization approach, we use several criteria. First, the registration is stopped when the maximum number of 100 iterations is reached or the step width of the algorithm turned subcritical. Therefore, we introduce the measure of the so-called *mean target point movement* (mTPM)

$$\mathrm{mTPM}^k = \frac{\sum_i w_i^k w_i^{k-1} (\hat{\mathbf{x}}_i^k - \hat{\mathbf{x}}_i^{k-1})^2}{\mathbf{w}^k \mathbf{w}^{k-1}}. \tag{7}$$

This measure gathers the distance between two corresponding target point sets in consecutive iterations while considering the weights assigned to each target point. When in a predefined number of iterations the mTPM is zero, registration is stopped.

A second criterion is applied to adapt the seek range of the algorithm. The seek range is dependant on the profile length L that is essential for local vessel detection. In the initial phase of the registration, the seek range has to be large to compensate for large misalignments, whereas in the final phase the seek range should be small to ensure a high matching accuracy. We use the following heuristic to progressively reduce the seek range according to the measured mean target point movement

$$L^k = \begin{cases} L_{\max} & k = 0 \\ \min\{L_{\min}, \frac{L^{k-1}}{2}\} & \mathrm{mTPM}^k < \epsilon \\ L^{k-1} & \text{otherwise.} \end{cases} \tag{8}$$

In our experiments, the initial, maximum seek range is arbitrarily set to $L_{\max} = 320$ pixels. The minimal profile length is set to $L_{\min} = 5$ pixels measured with respect to the detection plane. To ensure local convergence, the seek range is only reduced when the target point movement falls below a given limit ϵ.

4. RESULTS AND DISCUSSION

4.1 Validation with clinical data

According to[26], Fig. 7 shows the validation results obtained from the clinical data sets in form of scatter plots. For each registration experiment, the starting distance, which is the initial mTRE, is plotted against the resulting 3D projection error. The average 3D registration error computed for all experiments amounts to 6.43 mm for

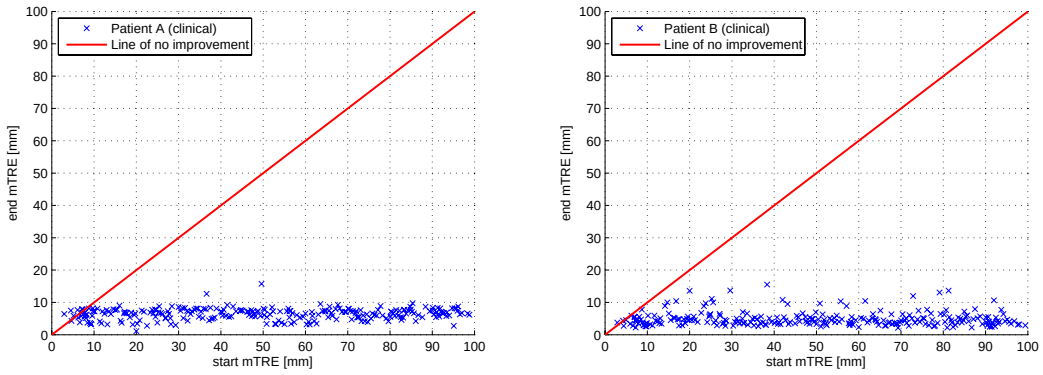

A **B**

Figure 7. Results of Monte-Carlo based validation with clinical data sets. Scatter plots for mTRE are obtained for clinical case A and B

case A and 4.91 mm for case B. Since no objective ground truth registration is available for these data sets, because they are clinical, no further quantitative measures of the registration quality are evaluated.

The accuracy of a typical registration result can visually be assessed in Fig. 5. Although matching ambiguities and different degrees of angiographic enhancement complicate the matching task, the projected 3D centerlines agree well with the target vessel trees as shown in the underlying DSA images. Especially in the distal parts but also in other parts of the vessel trees, the matching result is less accurate due to non-rigid deformations of the hepatic vessel tree induced by breathing, pulsatile blood flow or movements of the catheter.

These results indicate that the proposed registration algorithm is robust even for the boundary conditions of clinical data. In the Monte-Carlo study, the majority of experiments could largely improve the registration error given by the initial misalignment and robustly converged towards a certain accuracy level. In this study, the accuracy level depends on the manually defined reference registration. Furthermore, the results show that the visually optimal matching does not necessarily coincide with the matching the model-based registration computes. Further clinical validations have to show to which degree position differences to the reference registration and local misalignments are clinically significant.

4.2 Validation with synthetic data

Figure 8 shows the scatter plots of the validation results obtained from the synthetically generated data sets. For each registration experiment, the starting distance, which is the initial mTRE, is plotted against the resulting 3D projection error. In addition, the success rates for each of the 10 evaluation bins are presented in form of a bar graph. For case A, only one of the 250 experiments failed to register with a sufficient matching quality. Although this result exceeded the 5 mm success threshold it was far below the registration error given at the start. The average 3D registration error for all successful registrations amounts to 2.12 mm. According to the definition of the capture range in Sec. 3.3, for this case no limit of the capture range was found. Case B shows similar results. 13 registration experiments finished with a registration error higher than the 5 mm threshold. In 12 of these cases the starting distance of the initial misalignment could be reduced. The average registration error for all successful registrations is 2.18 mm. For this case, the capture range of our registration method ends at 40 mm.

In addition, the parameter configurations of all experiments that failed to stick to the accuracy limit were studied. In 9 of 14 cases, at least one of the rotation parameters in the starting configurations was larger than 10°.

These results proof that the proposed registration method is accurate and robust. Due to the large capture range of the proposed method, even extensive misalignments can be compensated. To our findings, the correction

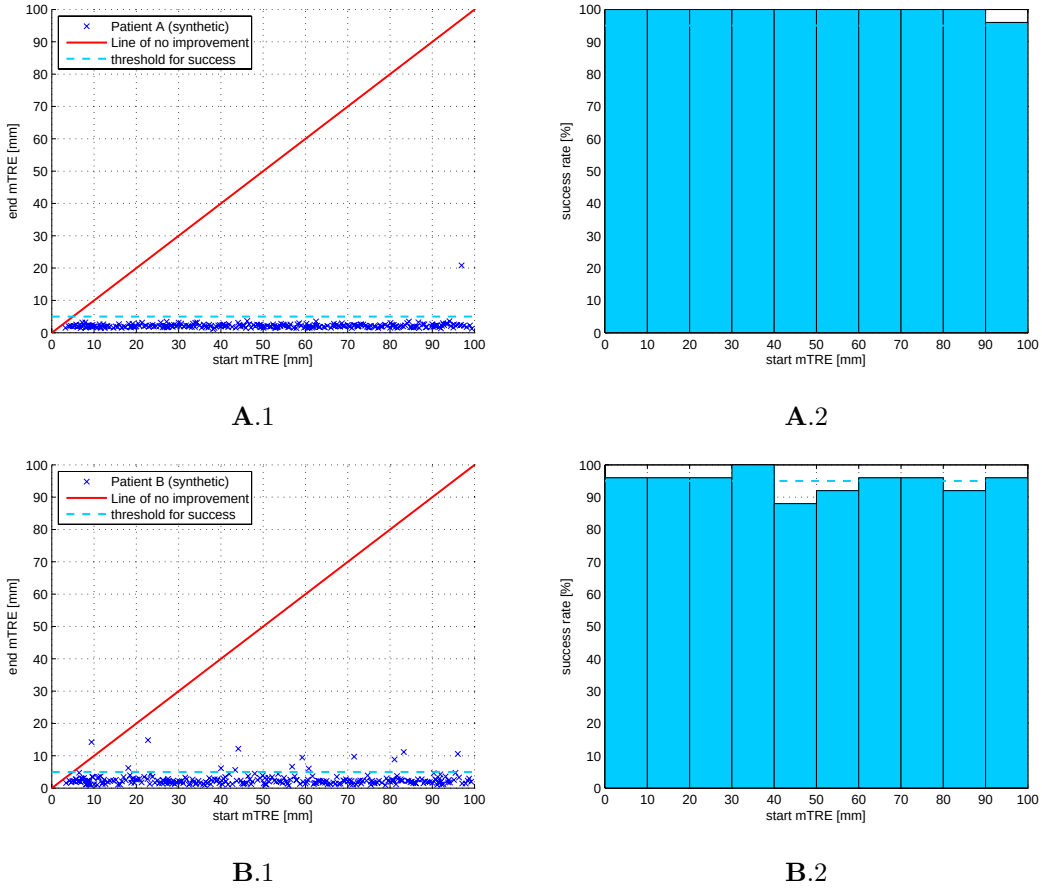

Figure 8. Registration results obtained from Monte-Carlo based validation with synthetically generated ground truth data. (**A.1**) scatter plot for mTRE, (**A.2**) success rates according to the 5 mm accuracy limit; (**B.1**) scatter plot for mTRE, (**B.2**) success rates according to the 5 mm accuracy limit

of the in-plane translations is easier than the optimization of the rotation parameters. Especially, when the initial misalignment caused by rotation exceeded 10° the registration quality decreases.

Furthermore, these results indicate that the registration quality may be dependant on the characteristics of the considered vessel tree and the chosen projection angle. The registration quality of the more complex case A is generally superior to the matching qualities of the less characteristic and more symmetrical case B. This may be due to the projection invariance inherent to typical vessel trees, which is described in more detail in[12]. In future, further simulation studies have to proof the accuracy and the reliability of the proposed registration method in the presence of noise and non-rigid deformations for a larger number of data sets.

5. CONCLUSIONS

A novel model-to-image based 2D-3D-registration approach for angiographic data was developed that combines well-known vessel detection techniques with aspects of model adaptation. Simulation studies and first experiments with clinical image data show that the proposed method is accurate and reliable. It was found that even large misalignments caused by the in-plane translations and 3D rotations can be compensated. Further effort has to be directed at correcting off-plane translation effects in an accurate and robust way. In future, this approach can be refined using further knowledge extracted from the reference centerline model as well as weighting vessel hierarchy and bifurcation distance for each centerline element separately. Moreover, higher flexibility in the registration can be obtained when allowing elastic deformations of single vessel segments.

6. ACKNOWLEDGMENTS

The authors would like to thank Associate Professor J. Geschwind and Assistant Professor K. Taguchi, Johns Hopkins hospital, Baltimore, for kindly providing the clinical image data. They would also like to thank D. Babic, Philips Medical Systems, Best, for the inspiring discussions.

REFERENCES

[1] Kerrien, E., Berger, M.-O., Maurincomme, E., Launay, L., Vaillant, R., and Picard, L., "Fully automatic 3D/2D subtracted angiography registration," in [*Medical Image Computing and Computer-Assisted Intervention – MICCAI'99*], *Lecture Notes in Computer Science* **1679**, 664–671 (1999).

[2] Hipwell, J., Penney, G., McLaughlin, R., Rhode, K., Summers, P., Cox, T., Byrne, J., Noble, J., and Hawkes, D., "Intensity-based 2-D–3-D registration of cerebral angiograms," *IEEE Transactions on Medical Imaging* **22**(11), 1417–1426 (2003).

[3] McLaughlin, R., Hipwell, J., Hawkes, D., Noble, J., Byrne, J., and Cox, T., "A comparison of a similarity-based and a feature-based 2-D–3-D registration method for neurointerventional use," *IEEE Transactions on Medical Imaging* **24**(8), 1058–1066 (2005).

[4] Chan, H. M., Chung, A. C. S., Yu, S. C. H., and Wells, W. M. I. I. I., "2D-3D vascular registration between digital subtraction angiographic (DSA) and magnetic resonance angiographic (MRA) images," in [*IEEE International Symposium on Biomedical Imaging: Macro to Nano*], 708–711 (2004).

[5] Dey, J. and Napel, S., "Targeted 2D/3D registration using ray normalization and a hybrid optimizer," *Medical Physics* **33**(12), 4730–4738 (2006).

[6] Florin, C., Williams, J., Khamene, A., and Paragios, N., "Registration of 3D angiographic and X-ray images using sequential monte carlo sampling," in [*Computer Vision for Biomedical Image Applications*], *Lecture Notes in Computer Science* **3765**, 427–436 (2005).

[7] Groher, M., Padoy, N., Jakobs, T. E., and Navab, N., "New CTA protocol and 2D-3D registration method for liver catheterization," in [*Medical Image Computing and Computer-Assisted Intervention – MICCAI 2006*], *Lecture Notes in Computer Science* **4190**, 873–881 (2006).

[8] Jomier, J., Bullitt, E., Horn, M. V., Pathak, C., and Aylward, S. R., "3D/2D model-to-image registration applied to TIPS surgery," in [*Medical Image Computing and Computer-Assisted Intervention – MICCAI 2006*], 662–669 (2006).

[9] Alperin, N., Levin, D. N., and Pelizzari, C. A., "Retrospective registration of X-ray angiograms with MR images by using vessels as intrinsic landmarks," *Journal of Magnetic Resonance Imaging* **4**(2), 139–144 (1994).

[10] Feldmar, J., Malandain, G., Ayache, N., Fernández-Vidal, S., Maurincomme, E., and Trousset, Y., "Matching 3D MR angiography data and 2D X-ray angiograms," in [*CVRMed-MRCAS'97*], *Lecture Notes in Computer Science* **1205**, 129–138 (1997).

[11] Kita, Y., Wilson, D. L., and Noble, J. A., "Real-time registration of 3D cerebral vessels to X-ray angiograms," in [*Medical Image Computing and Computer-Assisted Intervention – MICCAI'98*], *Lecture Notes in Computer Science* **1496**, 1125–1133 (1998).

[12] Liu, A., Bullitt, E., and Pizer, S., "3D/2D registration via skeletal near projective invariance in tubular objects," in [*Medical Image Computing and Computer-Assisted Intervention – MICCAI'98*], *Lecture Notes in Computer Science* **1496**, 952–963 (1998).

[13] Groher, M., Bender, F., Hoffmann, R.-T., and Navab, N., "Segmentation-driven 2D-3D registration for abdominal catheter interventions," in [*Medical Image Computing and Computer-Assisted Intervention – MICCAI 2007*], *Lecture Notes in Computer Science* **4792**, 527–535 (2007).

[14] Hill, D., Hawkes, D., and Hardingham, C., "Use of anatomical knowledge to register 3-D blood vessel data derived from DSA with MR images," in [*Medical Imaging V: Image Processing*], Loew, M., ed., *Proceedings of SPIE* **1445**, 348–357 (1991).

[15] Ecabert, O., Peters, J., Walker, A., von Berg, J., Lorenz, C., Vembar, M., Olszewski, M., and Weese, J., "Automatic whole heart segmentation in CT images: method and validation," in [*Medical Imaging 2007: Image Processing*], Pluim, J. and Reinhardt, J., eds., *Proceedings of SPIE* **6512**, 65120G (2007).

[16] Frangi, A., Niessen, W., Vincken, K., and Viergever, M., "Multiscale vessel enhancement filtering," in [*Medical Image Computing and Computer-Assisted Intervention – MICCAI'98*], *Lecture Notes in Computer Science* **1496**, 130–137 (1998).

[17] Deschamps, T. and Cohen, L., "Fast extraction of minimal paths in 3D images and applications to virtual endoscopy," *Medical Image Analysis* **5**(4), 281–299 (2001).

[18] Malandain, G., Bertrand, G., and Ayache, N., "Topological segmentation of discrete surfaces," *Int. Journal of Computer Vision* **10**(2), 183–197 (1993).

[19] Zahlten, C., Jürgens, H., Evertsz, C., Leppek, R., Peitgen, H.-O., and Klose, K., "Portal vein reconstruction based on topology," *European Journal of Radiology* **19**, 96–100 (1995).

[20] Gopal, A., Hoffmann, K., Rudin, S., and Bednarek, D., "Reconstruction of asymmetric vessel lumen from two views," in [*Medical Imaging 2002: Image Processing*], Sonka, M. and Fitzpatrick, J., eds., *Proceedings of SPIE* **4684**, 257–265 (2002).

[21] Chen, Z. and Molloi, S., "Vascular tree object segmentation by deskeletonization of valley courses," *Computerized Medical Imaging and Graphics* **26**(6), 419–428 (2002).

[22] Lorenz, C., Carlsen, I., Buzug, T., Fassnacht, C., and Weese, J., "Multi-scale line segmentation with automatic estimation of width, contrast and tangential direction in 2D and 3D medical images," in [*CVRMed-MRCAS'97*], *Lecture Notes in Computer Science* **1205**, 233–242 (1997).

[23] Levenberg, K., "A method for the solution of certain problems in least squares," *The Quarterly of Applied Mathematics* **2**, 164–168 (1944).

[24] Marquardt, D., "An algorithm for least-squares estimation of nonlinear parameters," *SIAM Journal on Applied Mathematics* **11**, 431–441 (1963).

[25] Waechter, I., Bredno, J., Barratt, D. C., Weese, J., and Hawkes, D. J., "Quantification of blood flow from rotational angiography.," in [*Medical Image Computing and Computer-Assisted Intervention – MICCAI 2007*], *Lecture Notes in Computer Science* **4791**, 634–641 (2007).

[26] van de Kraats, E., Penney, G., Tomaževič, D., van Walsum, T., and Niessen, W., "Standardized evaluation methodology for 2-D–3-D registration," *IEEE Transactions on Medical Imaging* **24**(9), 1177–1189 (2005).